

Neutron activation diagnostics at the National Ignition Facility (invited)

D. L. Bleuel, C. B. Yeaman, L. A. Bernstein, R. M. Bionta, J. A. Caggiano et al.

Citation: *Rev. Sci. Instrum.* **83**, 10D313 (2012); doi: 10.1063/1.4733741

View online: <http://dx.doi.org/10.1063/1.4733741>

View Table of Contents: <http://rsi.aip.org/resource/1/RSINAK/v83/i10>

Published by the [American Institute of Physics](#).

Related Articles

Calibration of neutron-yield diagnostics in attenuating and scattering environments
Rev. Sci. Instrum. **83**, 10D914 (2012)

Neutron field parameter measurements on the JET tokamak by means of super-heated fluid detectors
Rev. Sci. Instrum. **83**, 10E124 (2012)

Modulated active charge exchange fast ion diagnostic for the C-2 field-reversed configuration experiment
Rev. Sci. Instrum. **83**, 10D720 (2012)

Ultraviolet stimulated electron source for use with low energy plasma instrument calibration
Rev. Sci. Instrum. **83**, 073308 (2012)

Kinetic theory for charge-exchange spectroscopy: Effects of magnetic and electric fields on the distribution function after charge-exchange
Phys. Plasmas **19**, 072507 (2012)

Additional information on *Rev. Sci. Instrum.*

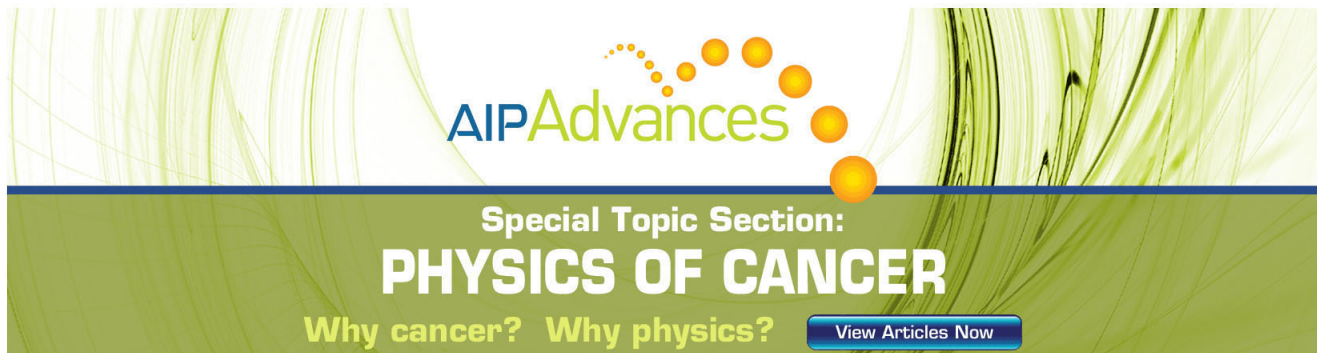
Journal Homepage: <http://rsi.aip.org>

Journal Information: http://rsi.aip.org/about/about_the_journal

Top downloads: http://rsi.aip.org/features/most_downloaded

Information for Authors: <http://rsi.aip.org/authors>

ADVERTISEMENT



AIP Advances

Special Topic Section:
PHYSICS OF CANCER

Why cancer? Why physics? [View Articles Now](#)

Neutron activation diagnostics at the National Ignition Facility (invited)^{a)}

D. L. Bleuel,^{1,b)} C. B. Yeaman,¹ L. A. Bernstein,¹ R. M. Bionta,¹ J. A. Caggiano,¹
 D. T. Casey,² G. W. Cooper,³ O. B. Drury,¹ J. A. Frenje,² C. A. Hagmann,¹ R. Hatarik,¹
 J. P. Knauer,⁴ M. Gatu Johnson,² K. M. Knittel,¹ R. J. Leeper,⁵ J. M. McNaney,¹ M. Moran,¹
 C. L. Ruiz,⁵ and D. H. G. Schneider¹

¹Lawrence Livermore National Laboratory, Livermore, California 94550, USA

²Massachusetts Institute of Technology Plasma Science and Fusion Center, Cambridge, Massachusetts 02139, USA

³University of New Mexico, Albuquerque, New Mexico 87131, USA

⁴Laboratory for Laser Energetics, University of Rochester, Rochester, New York 14623, USA

⁵Sandia National Laboratory, Albuquerque, New Mexico 87185, USA

(Presented 7 May 2012; received 7 May 2012; accepted 19 June 2012;
 published online 9 August 2012)

Neutron yields are measured at the National Ignition Facility (NIF) by an extensive suite of neutron activation diagnostics. Neutrons interact with materials whose reaction cross sections threshold just below the fusion neutron production energy, providing an accurate measure of primary unscattered neutrons without contribution from lower-energy scattered neutrons. Indium samples are mounted on diagnostic instrument manipulators in the NIF target chamber, 25–50 cm from the source, to measure 2.45 MeV deuterium-deuterium fusion neutrons through the $^{115}\text{In}(n,n')^{115\text{m}}\text{In}$ reaction. Outside the chamber, zirconium and copper are used to measure 14 MeV deuterium-tritium fusion neutrons via $^{90}\text{Zr}(n,2n)$, $^{63}\text{Cu}(n,2n)$, and $^{65}\text{Cu}(n,2n)$ reactions. An array of 16 zirconium samples are located on port covers around the chamber to measure relative yield anisotropies, providing a global map of fuel areal density variation. Neutron yields are routinely measured with activation to an accuracy of 7% and are in excellent agreement both with each other and with neutron time-of-flight and magnetic recoil spectrometer measurements. Relative areal density anisotropies can be measured to a precision of less than 3%. These measurements reveal apparent bulk fuel velocities as high as 200 km/s in addition to large areal density variations between the pole and equator of the compressed fuel.

© 2012 American Institute of Physics. [<http://dx.doi.org/10.1063/1.4733741>]

I. INTRODUCTION

An accurate measurement of the neutron yield and the capsule fuel areal density (ρR) of inertial confinement fusion implosions at the National Ignition Facility (NIF) (Ref. 1) is essential to evaluate its performance on the experimental path to achieve ignition.^{2,3} Neutron yield is directly proportional to the number of fusion reactions while the areal density measures the degree of compression achieved. Furthermore, measurement of a complete ρR distribution over all angles indicates the compression entropy, drive anisotropy, and lower-order mix which may impede ignition.

Activation foils have long been used to measure neutron fluence and spectra for a variety of neutron sources, including inertial confinement fusion facilities such as OMEGA.⁴ A chosen sample of material undergoes nuclear reactions upon exposure to neutrons above a certain energy threshold, creating a radioactive species. The subsequent decay of the radioactive nuclei can be measured and the number of neutrons passing through the material can be deduced. For an isotropic, instantaneous neutron source, the unscattered neutron yield, Y ,

above a reaction's energy threshold is calculated as

$$Y = \frac{4\pi R^2 A N_c}{m f_{BR} f_a N_A \varepsilon_i \varepsilon_d \langle \sigma \rangle e^{-\lambda(\Delta t_s)} [1 - e^{-\lambda(\Delta t_c)}]}, \quad (1)$$

where R is the distance from the neutron source to the activation sample, A is the atomic mass of the isotope undergoing the reaction of interest, N_c is the number of decay particles or gamma rays measured in a detector, m is the mass of the sample, f_{BR} is the branching ratio producing the detected radiation, f_a is the abundance of the isotope in the sample (including sample purity), N_A is Avogadro's number, ε_i is the irradiation efficiency (a deviation from unity indicating neutron absorption or scattering from environmental materials and in the sample itself), ε_d is the detection efficiency, $\langle \sigma \rangle$ is the spectrum-weighted cross section, λ is the decay constant of the radioactive material, Δt_s is the time between the irradiation and start of measurement, and Δt_c is the time over which radiation from the sample is measured.

At the NIF, to measure both neutron yield and implosion areal density variations, $\rho R(\Omega)$, neutron activation diagnostics (NADs) (Ref. 5) are implemented with five different methods, named for their deployment locations: Well-NAD, NAD20, DIM-NAD, Snout-NAD, and Flange-NAD. Indium is used to measure 2.45 MeV neutrons produced from deuterium-deuterium (D-D) fusion reactions while both zirconium and copper are used to measure 14 MeV neutrons

^{a)}Invited paper, published as part of the Proceedings of the 19th Topical Conference on High-Temperature Plasma Diagnostics, Monterey, California, May 2012.

^{b)}Author to whom correspondence should be addressed. Electronic mail: bleuel1@llnl.gov.

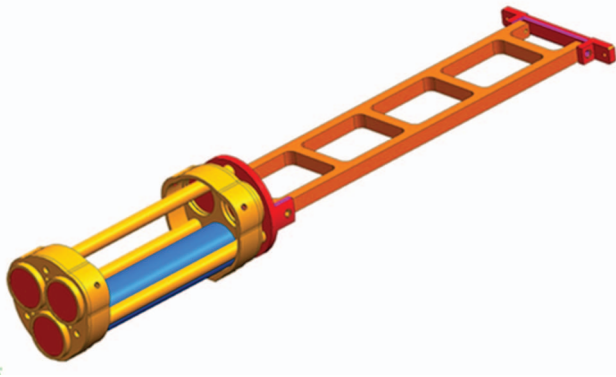


FIG. 1. Well-NAD insertion apparatus drawing.

from deuterium-tritium (D-T) reactions. As the thickness of these samples is generally 1 mm or greater, the nomenclature used here of “foil” is more historical than descriptive.

Presented here is a summary and status update of the different activation methods at NIF and some representative results. The full analysis details and results for the past several years of NIF shots will be covered in forthcoming publications.

II. WELL-NAD

Three zirconium foils of 1 mm, 3.5 mm, and 8.7 mm respective thicknesses are deployed in a diagnostic “well,” on the NIF chamber at the (θ, ϕ) coordinates of (64,241), where $\theta = 0^\circ$ is the top of the chamber. The well allows insertion of the zirconium to 4.48 m from the capsule implosion, in front of the inside first wall of the chamber to minimize small-angle neutron scatter into the foils, but outside the chamber vacuum for easy retrieval. Three additional foils may optionally be deployed 40 cm behind the primary set, with one foil blocked by a tungsten “shadowbar” for background measurements. However, due to retrieval difficulties, operation with the shadowbar is not currently permitted. This insertion apparatus is shown in Figure 1. Neutrons from D-T fusion undergo $^{90}\text{Zr}(n,2n)^{89}\text{Zr}$ reactions in each sample while lower energy neutrons below the 12.1 MeV threshold do not react. A small <2% contribution to activation, currently included only in the uncertainty, is predicted from fuel-scattered neutrons above this threshold. The ^{89}Zr product then $\beta+$ decays with a 3.27 day half life to $^{89\text{m}}\text{Y}$, emitting a 909.0 keV gamma ray several seconds later. These gamma rays are measured using lead-shielded high-purity germanium detectors in a low-background counting facility. A 5.7% overall reduction in sample activation due to absorption in the 1 cm thick wall of the well and scatter in surrounding materials (ε_i in Eq. (1)) was estimated with a Monte Carlo simulation using MCNP6 (Ref. 6) and corrected for. This correction is dominated by the attenuation of neutrons in the well wall. The $^{90}\text{Zr}(n,2n)$ cross section is very well known, to less than 1% uncertainty around 14 MeV.⁷ Assuming a Gaussian neutron spectrum centered at 14.028 MeV with a full width at half maximum of 350 keV, the spectrum-weighted cross section, $\langle\sigma\rangle$, is 596 mb, including contributions from $^{90}\text{Zr}(n,2n)^{89\text{m}}\text{Zr}$ reactions decaying to

TABLE I. Typical Well-NAD uncertainties for thick (8.7 mm) zirconium samples.

Quantity	Effect on activity (%)	Uncertainty in yield (%)
Detector efficiency		5
Gamma-ray self-shielding (SS)	-15	(incl. above)
Neutron “depletion” in Zr		0.6
SS differential from n depletion	-3.1	2.0
$^{90}\text{Zr}(n,2n)$ cross section		1.0
Position relative to implosion		<1
Scatter/Absorption off well	-5.7	1.1
Chamber/wall scatter		<1
Non-primary neutrons		2.0
Velocity/temperature peak shift		2.0
Ion temperature peak broadening		<1
Sample purity	-1.35	0.2
Sample weight/contamination		<1
Counting statistics ($Y_n > 10^{14}$)		1-2

the ^{89}Zr ground state with a 4.161 min half life. This differs only slightly from the value of 595 mb for monoenergetic neutrons at 14.028 MeV, demonstrating a high insensitivity to the spectral width, broadened by the capsule fuel ion temperature. Uncertainties in each parameter of Eq. (1) contribute to an overall yield uncertainty of about 7%, dominated by uncertainties in the detector calibration and counting geometry corrections (estimated as 5%) and are tabulated in Table I.

It is expected that improved detector characterization will lower this contribution to 3% (limited by a NIST-traceable calibration source uncertainty of 2%), achieving a best total yield uncertainty of $\sim 5\%$.

III. NAD20

The NAD20 diagnostic was named for its proximity to the “nToF20” neutron time-of-flight diagnostic, itself located about 20 m from the target chamber center in the “neutron alcove”. Two copper foils, respectively, 1 mm thick and 9.5 mm thick, are deployed both in front of the nToF20 detector array at 19 m from the implosion (NAD19) and behind (NAD29) the array at 29 m from the source in a well-shielded room. Neutrons from D-T fusion activate the copper samples via the $^{63}\text{Cu}(n,2n)^{62}\text{Cu}$ reaction with an 11.0 MeV threshold, which subsequently decays by gammaless $\beta+$ emission. Because of the short 9.67 min half life of ^{62}Cu , the samples must be retrieved and measured quickly. The 180° -opposed 511 keV gamma rays from annihilation of the emitted positron are detected in coincidence by two back-to-back NaI detectors, between which the sample is inserted within 30 min of irradiation. The competing $^{65}\text{Cu}(n,2n)^{64}\text{Cu}$ reaction also decays by positron emission but with a 12.7 h half life and its small contribution over short time scales is measured and subtracted. The yield uncertainty, of the closest copper sample is typically $\sim 8\%$. Further details are described elsewhere, including in these proceedings.⁸⁻¹⁰

Generally, yields determined by all three Well-NAD zirconium foils and both copper foils agree with each other

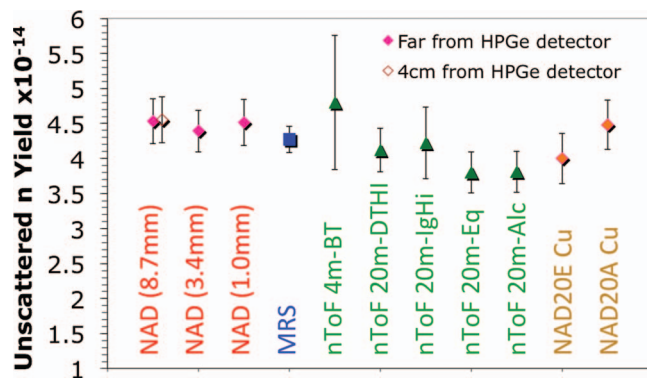


FIG. 2. Unscattered DT neutron yields as measured from different diagnostics on NIF shot N120417-001, a layered-cryogenic D-T shot. Well-NAD results (red, leftmost) are shown for the thickest sample when the sample was counted both close to and far from the detector. NAD20 results (orange, right) are from copper foils on the equator (E) at (90,174) and in the alcove (A) at (116,315).

and with the other yield diagnostics: the magnetic recoil spectrometer (MRS) (Ref. 11–16) and a variety of nToF detectors.^{17–19} An example is shown for a representative shot in Figure 2. The nToF detectors themselves are calibrated to a weighted average of these activation foils and the MRS on previous shots, however, and their agreement with these diagnostics is therefore demonstrative only of relative shot-to-shot consistency.

IV. DIM-NAD AND SNOOT-NAD

Indium samples between 1–5 mm thick can be deployed two ways inside the NIF chamber to measure 2.45 MeV D-D neutrons. When mounted on the centerline of the end of a diagnostic instrument manipulator (DIM), it is designated DIM-NAD. An indium holder was designed to attach to one of two other diagnostics, known as GXD and VISAR, depending on which of those diagnostics were last mounted on the DIM. When a DIM is otherwise in use, indium may be attached on the side of a DIM in a “Snout” normally used for the wedge range filter (WRF) diagnostic, either behind the WRF components or alone.

The $^{115}\text{In}(n,n')^{115\text{m}}\text{In}$ cross section rises rapidly between 1–2 MeV and remains relatively constant across the region around 2.45 MeV, making it relatively insensitive to ion temperature or scattered neutrons below ~ 1 MeV. The $^{115\text{m}}\text{In}$ isomer emits 336.2 keV gamma rays with a 4.486 h half life. These gamma rays are measured in the same low-background counting facility described in Sec. II. Due to low neutron yields and a higher scattered-neutron sensitivity, indium activation must occur very close to the implosion with little shielding. The yield uncertainty when placed 50 cm from the target, enumerated similarly to that of zirconium, is typically $\sim 10\%$. The $^{115}\text{In}(n,n')^{115\text{m}}\text{In}$ cross section from IRDF-90 (Ref. 20) was used as it agrees better with experimental data in the literature than other evaluations. A higher cross section uncertainty of 5% was assigned because of these literature and evaluated library differences. A scatter/absorption correction of -11% for DIM-NAD and -4.4% for Snout-NAD

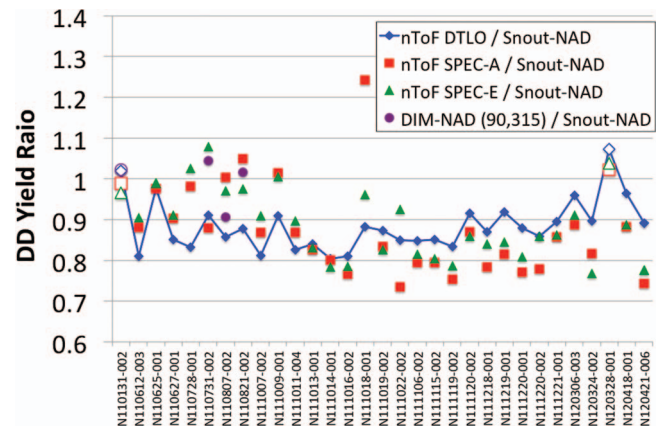


FIG. 3. Ratio of nToF-measured (and DIM-NAD when available) DD yields to Snout-NAD yields. Open symbols on N110131-002 and N120328-001 represent exploding pushers. For clarity, uncertainties are not shown but are on order of 12%–14%, of which more than half is systematic, common to the exploding pusher cross-calibration.

is applied to the measured yield based on MCNP (Ref. 6) simulations of the DIM and mount geometry.

Curiously, the D-D yield on symmetric capsule (Sym-Cap) and convergent ablation (ConA) implosions has consistently differed from that of nToF detectors by about 15%, even though the nToF detectors were calibrated to indium activation on an exploding pusher shot (N110131-002). The difference is particularly evident when comparing to the nToF-DTLO detector, which has not undergone significant equipment alterations or changes in analysis methods over the duration of measurements. To investigate this systematic difference, shown in Figure 3, a second exploding pusher shot (N120328-001) was fired with four Snout-NAD indium samples (two at 90,78 and two at the north pole). The nToF diagnostics agreed within uncertainties with all four indium activations on this shot, suggesting a physical difference between exploding pushers and SymCap/ConA shots. The lower threshold of the $^{115}\text{In}(n,n')^{115\text{m}}\text{In}$ cross section relative to the 2.45 MeV D-D neutrons make it more sensitive to environmental neutron scatter than Well-NAD, though MCNP (Ref. 6) simulations suggest that scatter off diagnostics not present on exploding pushers is not likely to explain the large observed discrepancy. The effect of downscattered neutrons off fuel and hohlraum is currently being investigated.

V. FLANGE-NAD

A. Fuel areal density

In a cryogenic layered capsule shot, there is a significant areal density (ρR) of cold fuel compressed throughout the fusion burn time. A significant percentage of primary 14 MeV neutrons scatter in this dense layer and lose enough energy to fall below the zirconium or copper cross section energy thresholds. Thus, it is understood that the absolute yield measurements are actually only measurements of the unscattered primary D-T neutrons. Other diagnostics, such as the nToF detectors and the MRS, provide spectral information and attempt to measure a portion of these scattered neutrons in ratio

to the unscattered yield to infer the ρR along a specific line of sight. In a perfectly symmetric capsule compression, this “downscattered ratio” and the yield would be independent of angle. However, anisotropies in the ρR will differentially reduce the primary unscattered yield along different lines of sight as neutrons pass through variant- ρR zones. The scattered yield, on the other hand, will increase along specific energy-dependent angles to their original path.¹¹ To measure anisotropies in the yield, and therefore the capsule $\rho R(\Omega)$ as a function of angle, Ω , thick zirconium foils were placed on the outside of nine selected “flanges” (unused diagnostic port covers) around the chamber. The (θ, ϕ) coordinates of these nine flanges are: (7,0); (64,39); (64,111); (64,200); (90,45); (90,123); (90,213); (102,144); and (161,236). After February 2012, seven more foils were added on flanges at coordinates: (7,180); (18,213); (36,356); (64,292); (90,303); (116,200); and (143,176). Including the Well-NAD location (64,241), this provides 17 well-distributed measurements of relative unscattered yield around the chamber.

All foils are measured sequentially in the same detector in the same geometry to eliminate relative systematic uncertainties. By normalizing the activity from each flange position to that from the same flange measured in an assumed-isotropic exploding pusher shot and observing flange-to-flange differences in ratio to the reference zirconium sample from the Well-NAD measurement (also measured in the same detector and geometry), all uncertainties except for counting statistics are minimized down to as low as 2%–3%. This double ratio of angular-dependent unscattered yields, $Y(\Omega)$, is derived from Eq. (1) as the specific activity ratio, R_{SA} ,

$$R_{SA} = \frac{Y_A(\Omega_1)/Y_A(\Omega_2)}{Y_B(\Omega_1)/Y_B(\Omega_2)} = \left(\frac{m_{A2}m_{B1}}{m_{A1}m_{B2}} \right) \left(\frac{A_{A1}^0}{A_{A2}^0} \right) \left(\frac{A_{B2}^0}{A_{B1}^0} \right), \quad (2)$$

where the A and B subscripts designate, respectively, the layered cryogenic shot of interest and the isotropic exploding pusher; the 1 and 2 subscripts designate, respectively, the flange of interest and the reference sample (from Well-NAD); m is the mass of each sample and A^0 is the activity of each sample at the time of irradiation. The uncertainties in the masses are extremely small compared to that from the counting statistics.

The unscattered yield at a given angle relates to the primary fusion yield, Y_p , (before scattering in the fuel) by the relation

$$Y(\Omega) = Y_p e^{-\rho R(\Omega)\langle\sigma_{DT}\rangle/m_{DT}}, \quad (3)$$

where, for a 50/50 mix of deuterium and tritium, $\langle\sigma_{DT}\rangle$ is the averaged spectrum-weighted cross section for neutron interactions with deuterons and tritons and m_{DT} is the average mass of a deuteron and triton. Here, $\rho R(\Omega)$ is used as shorthand for the more formal $\rho(\Omega)R(\Omega)$. Assuming a constant $\rho R(\Omega)$ for a calibration shot, B , the double ratio from Eq. (2) becomes

$$\frac{Y_A(\Omega_1)/Y_A(\Omega_2)}{Y_B(\Omega_1)/Y_B(\Omega_2)} = \frac{e^{-\rho R(\Omega_1)\langle\sigma_{DT}\rangle/m_{DT}}}{e^{-\rho R(\Omega_2)\langle\sigma_{DT}\rangle/m_{DT}}}. \quad (4)$$

Then, choosing a reference Ω_2 (the Well-NAD sample at 64,241) such that $\rho R(\Omega_1) = \rho R(\Omega_2) + \Delta[\rho R(\Omega_1)]$, we can

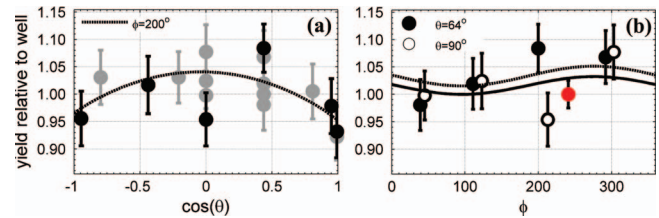


FIG. 4. Activation ratio for shot N120205–002 as a function of (a) polar and (b) azimuthal angle. Black datapoints in (a) are roughly along the $\theta = 200^\circ$ axis. The red circle in (b) is the reference Well-NAD measurement (set to unity). Lines represent the fits in Figure 5, with the dashed and solid lines in (b) respectively the fit values along the $\theta = 90^\circ$ and $\theta = 64^\circ$ axes.

relate the absolute increase in $\rho R(\Omega_1)$ over the value at Ω_2 as

$$\Delta[\rho R(\Omega_1)] = -\frac{m_{DT}}{\langle\sigma_{DT}\rangle} \ln [R_{SA}]. \quad (5)$$

Using ENDF/B-VIII (Ref. 21) cross section values of 809 mb and 948 mb, respectively, for neutron interactions with deuterium and tritium at 14.03 MeV, the quantity $m_{DT}/\langle\sigma_{DT}\rangle$ is 4.75 g/cm². Thus, an 18% decrease in measured activity from one position to the reference equates to a 1 g/cm² increase in ρR along that line of sight. Such an increase is of the same magnitude as the ρR values inferred from current downscattered ratio measurements by nToF and MRS. In other words, an observed 18% decrease in the specific activity ratio represents a near doubling of the ρR along that line of sight. An example of this specific activity ratio, showing such a significant effect on the poles, is plotted for one particular NIF shot in Figure 4.

A least-squares fit to a physically-relevant model of areal density can help to predict the change in ρR along lines of sight lacking activation foils. Such an “activation map” is shown in Figure 5 for the same example shot, in which the data were fit only to the three first spherical harmonics and the polar-symmetric second spherical harmonic. Areal density oblateness (higher ρR at the poles) is typical of all layered-cryogenic NIF shots to date. A recent investigation of in-chamber interferences has shown small line-of-sight neutron blockages of the two north polar samples by the end cap of the polar HGXI diagnostic. Low polar activation is observed both in blocked and unblocked configurations, suggesting only a partial effect. However, the full contribution of diagnostic interferences must be determined and subtracted. The data in Figures 4 and 5 represent an unblocked configuration according to engineering drawings, though the line of sight to the topmost samples cleared the HGXI end cap by only a few millimeters and thus minor experimental deviations from those specifications must be considered.

In principle, Figure 5 could be converted into an absolute $\rho R(\Omega)$ map by performing a $\Delta[\rho R(\Omega)]$ fit using Eq. (5) and adding it to an independent measurement of the ρR along a given line of sight. However, the MRS and nToF diagnostics measure the ratio of downscattered neutrons from 10–12 MeV to the unscattered 13–15 MeV neutrons which reach those detectors. The scattered neutrons originate along different lines of sight from the axis of the unscattered neutrons. Conversion of this downscattered ratio to ρR requires an assumption of isotropy. Efforts are underway to use Flange-NAD results to

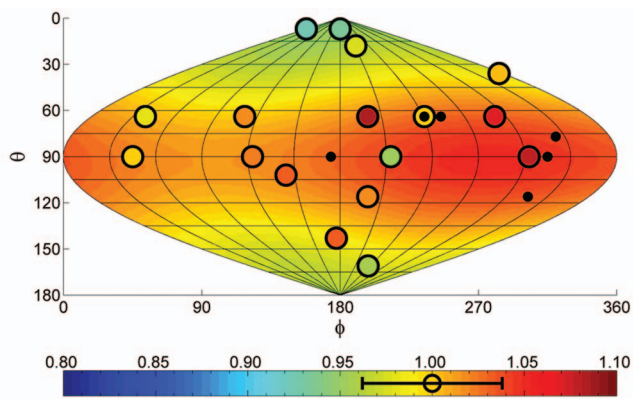


FIG. 5. Activation ratio (R_{SA}) datapoints (open circles) from Figure 3 with a fit to low-order spherical harmonics (see text). Solid dots indicate positions of nToF and MRS (77,324) diagnostics. The fit uncertainty is shown in the colorbar.

predict relative downscattered ratio measurements and positive correlations are already apparent.

Additionally, neutrons may be scattered by remaining plastic ablator mass rather than DT fuel, with different scattering masses and cross sections. This contribution is under investigation and must be differentiated before a final quantitative determination of fuel ρR may be made.

B. Bulk fuel velocity

If an imploding capsule is moving with a high velocity relative to the chamber, the deuterium and tritium reactants may fuse with a higher average energy along the line of sight of bulk motion. Because the cross section of zirconium (or copper) increases roughly linearly at 14 MeV, this will result in an increase in activation along the bulk velocity axis and a corresponding decrease in the opposite direction. This effect may be misinterpreted as areal density variations. Such velocities have been correlated with “dropped quads” (non-operational lasers in packs of four) and misaligned targets.

To some extent, velocity can be identified by its dipole nature on a large coverage of activation foils. However, it may also be characterized by neutron energy peak shifts in the MRS and nToF spectral measurements along their given lines of sight. By an integrated analysis of all these diagnostics, bulk velocities as high as 200 km/s have been observed on exploding pusher shots with much lower velocities on layered-cryogenic shots. This has somewhat complicated Flange-NAD calibration efforts. The data presented in Figures 4 and 5, for instance, were normalized to a 17-foil exploding pusher (N120217-001) with an apparent velocity of 165 ± 71 km/s along the (86,319) axis, as compared to a previous low-velocity 10-foil calibration shot (N111121-003). This velocity was fit and then subtracted from the calibration data, resulting in larger uncertainties. Final calibration of the seven locations added after February 2012 is awaiting a future high-yield, low-velocity exploding pusher.

A full analysis of the observation of bulk fuel velocity will be addressed in a forthcoming publication. An *in situ* variant on the Flange-NAD diagnostic using a co-located, higher-thresholding reaction such as $^{39}\text{K}(n,2n)$

may be implemented²² to directly measure velocity components along each line of sight.

VI. SUMMARY

Utilization of a suite of activation diagnostics has provided high-accuracy, independent measurements of yield along multiple lines of sight for relatively minimal cost and effort. Excellent agreement among multiple diagnostics lends high confidence to D-T yield measurements. Small discrepancies between D-D yield diagnostics on SymCap and ConA shots are being investigated. Significant anisotropies in ρR on some shots are being observed by activation foils in multiple locations around the NIF chamber. Large bulk fuel center-of-mass velocities on order of 100 km/s are regularly observed on exploding pusher shots.

ACKNOWLEDGMENTS

We would like to extend a special thanks to LLNL’s Nuclear Counting Facility and its personnel, especially Cindy Conrado, Todd Wooddy, Bryan Bandong, and Phil Torretto. This work performed under the auspices of the (U.S.) Department of Energy by Lawrence Livermore National Laboratories and Sandia National Laboratories under Contract Nos. DE-AC52-07NA27344 and DE-AC04-94AL85000.

¹E. I. Moses, *Fusion Sci. Technol.* **44**, 11 (2003).

²J. D. Lindl, *Inertial Confinement Fusion: The Quest for Ignition and Energy Gain using Indirect Drive*. (Springer, New York, NY, USA, 1998).

³M. J. Edwards *et al.*, *Phys. Plasmas* **18**(5), 051003 (2011).

⁴T. R. Boehly *et al.*, *Opt. Commun.* **133**(1–6), 495–506 (1997).

⁵D. L. Bleuel *et al.*, in the *Proceedings of 7th International Conference on Inertial Fusion Science and Applications, Bordeaux-Lac, France, 2011* (European Physical Journal: Web of Conferences, Les Ulis Cedex A, France, in press).

⁶T. Goorley *et al.*, Los Alamos National Laboratory LA-UR-11-05198, Nuclear Technology (in press).

⁷A. Pavlik, G. Winkler, H. Vonach, A. Paulsen, and H. Liskien, *J. Phys. G* **8**, 1283 (1982).

⁸G. W. Cooper *et al.*, “Copper activation total DT neutron yield measurements at the National Ignition Facility,” *Rev. Sci. Instrum.* (these proceedings).

⁹G. W. Cooper and C. L. Ruiz, *Rev. Sci. Instrum.* **72**, 814 (2001).

¹⁰R. J. Leeper *et al.* in *Proceedings of 7th International Conference on Inertial Fusion Science and Applications, Bordeaux-Lac, France, 2011* (European Physical Journal: Web of Conferences, Les Ulis Cedex A, France, in press).

¹¹M. Gatu Johnson *et al.*, “Neutron spectrometry—An essential tool for diagnosing implosions at the National Ignition Facility,” *Rev. Sci. Instrum.* (these proceedings).

¹²D. T. Casey *et al.*, “Measuring the absolute DT neutron yield using the Magnetic Recoil Spectrometer at OMEGA and the NIF,” *Rev. Sci. Instrum.* (these proceedings).

¹³J. A. Frenje *et al.*, *Rev. Sci. Instrum.* **72**, 854 (2001).

¹⁴J. A. Frenje *et al.*, *Rev. Sci. Instrum.* **79**, 10E502 (2008).

¹⁵J. A. Frenje *et al.*, *Phys. Plasmas* **17**, 056311 (2010).

¹⁶D. T. Casey *et al.*, *Rev. Sci. Instrum.* **82**(7), 073502 (2011).

¹⁷V. Yu. Glebov *et al.*, *Rev. Sci. Instrum.* **81**, 10D325 (2010).

¹⁸C. Stoeckl, M. Cruz, V. Yu. Glebov, J. P. Knauer, R. Lauck, K. Marshall, C. Mileham, T. C. Sangster, and W. Theobald, *Rev. Sci. Instrum.* **81**, 10D302 (2010).

¹⁹Z. A. Ali *et al.*, *Rev. Sci. Instrum.* **79**, 10E527 (2008).

²⁰N. P. Kocherov and P. K. McLaughlin, “The International Reactor Dosimetry File, IRDF-90 Version 2,” IAEA-NDS-141, Rev. 2 (1993).

²¹CSEWG-Collaboration, Evaluated Nuclear Data File ENDF/B-VI.8, www.nndc.bnl.gov/endl, as of May 7, 2012.

²²C. B. Yeamans, D. L. Bleuel, and L. A. Bernstein, “Enhanced NIF neutron activation diagnostics,” *Rev. Sci. Instrum.* (these proceedings).